Direct Detection of Pilot Carrier-Assisted DMT Signals with Pre-Phase Compensation and Imaginary Noise Suppression

Zhenrong Zhang, Jianping Li, Yuncai Wang, and Yunwen Qin

***Abstract*—We propose and experimentally demonstrate a cost-effective pilot carrier assisted direct detection scheme based on discrete multitone (DMT) modulation format. The cost of the proposed scheme can be substantially reduced by two ways. First, we use distributed feedback (DFB) laser with large linewidth (~10 MHz) as the pilot carrier. Secondly, we design a low-complexity pre-phase compensation (PPC) algorithm combined with imaginary noise suppression (INS), in order to mitigate the effect of phase noise and consequently enhance the signal to noise ratio (SNR). Different from conventional channel equalization schemes for the DMT signal, we pre-compensate the phase noise in time domain before fast Fourier transform (FFT) demodulation at the receiver side. The PPC algorithm is implemented with an average operation, instead of complex multipliers. Since DMT signal is a real-valued signal, the imaginary part of time-domain samples after the PPC process is only noise, which can be removed for the SNR enhancement. Simulation results indicates that 3-dB SNR improvement can be obtained, which agrees well with the theoretical analysis. Meanwhile, our experimental results show that the combination of PPC and INS can significantly improve the laser linewidth tolerance of transmission system, leading to the possible use of DFB laser, instead of external cavity laser (ECL), as the pilot carrier. Finally, we successfully demonstrate 4×50-Gb/s DMT signal transmission over 400-km standard single mode fiber (SSMF) by using DFB lasers as signal and pilot carriers, respectively, with sufficient margin to reach 20% forward error correction (FEC) threshold.**

***Index Terms*— discrete multitone (DMT), fast Fourier transform (FFT), pre-phase compensation (PPC), imaginary noise suppression (INS).**

I. INTRODUCTION

THE demand for low-cost and high-speed per-wavelength data transmission becomes urgent, due to the fast development of 5G and cloud computing [1, 2]. In comparison with coherent detection, direct detection is more suitable for the scenarios of datacenter photonic interconnection and metropolitan network at the range between 100 km and 400 km. The main challenge direct detection scheme encounters is that the transmission distance is limited because of the chromatic dispersion (CD) induced power fading at C-band and commercial unavailability of cost-effective optical amplifier at O-band. In order to extend the transmission distance based on direct detection scheme, optical single sideband (OSSB) modulation has been reported as the most effective method to overcome the CD-induced power fading effect. The OSSB signals can be generated in optical domain by optical filtering [3, 4] and in digital domain by digital pre-processing with complex IQ modulation [5, 6]. In the direct detection scheme, the single-wavelength data rate can achieve 100 Gb/s or 200 Gb/s after optical filtering or IQ modulator, with transmission distance up to 100 km and 1200 km, respectively [3, 5]. However, the use of optical filter and IQ modulator may either increase the power loss or reduce the effective signal-to-noise ratio (SNR). In addition, current optical transmission products with direct detection are usually based on direct laser modulation or intensity modulation. Therefore, these schemes may significantly change the structure of optical transmission link, leading to a huge increase of the total cost.

Recently, pilot carrier-assisted direct detection based on pulse amplitude modulation (PAM) have been proposed and experimentally demonstrated [7]. By combining another laser source with the optical signal at the transmitter side, the optical field of the signal is completely reserved after the beating between the optical signal and the additional laser source at the photodetector (PD), where the additional laser source acts as a pilot carrier. Therefore, almost all optical components in the current direct detection schemes can be reused with only small modifications of transmitter configuration. In addition, digital signal processing (DSP) algorithms like digital carrier regeneration (DCR) and pre-phase compensation (PPC) have been proposed to mitigate the phase noise of PAM signal [8-10]. As a result, low-cost laser with large linewidth can be applied in the pilot carrier-assisted signal transmission scheme for system cost reduction. However, previous DSP algorithms

Manuscript received XX; revised XX. This work was supported in part by the National Key R&D Program of China (2018YFB1801001), National Natural Science Foundation of China (62022029, 61875061, 61661004), and Guangxi Science Foundation (2017GXNSFAA198227), in part by the Program for Guangdong Introducing Innovative and Enterpreneurial Teams (2019ZT08X340), and in part by the Research and Development Plan in Key Areas of Guangdong Province (2018B010114002). (Corresponding author: jianping@gdut.edu.cn).

Zhenrong Zhang is with the Guangxi Key Laboratory of Multimedia Communications and Network Technology, School of computer, electronics and information, Guangxi University, Nanning 530004, China.

Jianping Li, Yuncai Wang, and Yuwen Qin are with Advanced Institute of Photonics Technology, School of Information Engineering, Guangdong University of Technology, and also with Guangdong Provincial Key Laboratory of Photonics Information Technology, Guangzhou, 510006, China.

for phase noise mitigation require either large size fast Fourier transformation (FFT) [8, 9] or linear digital filter with large number of taps [10], leading to high computational complexity.

In this paper, we apply discrete multi-tone (DMT) modulation format [11, 12] for the pilot carrier-assisted direct detection scheme. Regarding to the characteristic of DMT signal, a low-complexity PPC algorithm is designed to mitigate the laser phase noise. In comparison with the previously proposed DCR or PPC algorithms, there occurs almost no additional computational complexity in terms of complex multiplier operation for the phase noise mitigation. Since DMT signal is real-valued signal, we can remove the imaginary part of signal after PPC to further enhance the SNR. Finally, our proposed method is experimentally verified with performance enhancement due to the use of low-complexity PPC and imaginary noise suppression (INS), especially when a cheap DFB laser with a linewidth of ~10MHz is used. A net total data rate of 4×50 Gb/s optical DMT signals can be successfully transmitted over 400-km standard single mode fiber (SSMF), based on our proposed pilot carrier-assisted direct detection scheme.

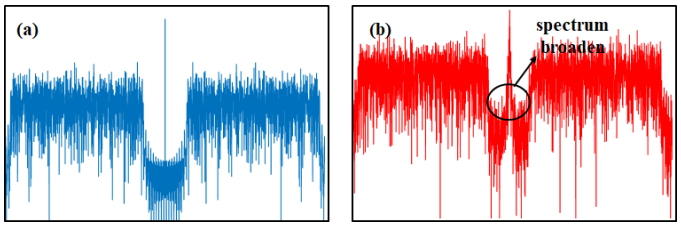

Fig. 1 Simulated optical spectrum of DMT signal (a) without laser phase noise and (b) with laser phase noise.

II. Operation Principle

Although DMT signal is real-valued signal, the imaginary part is introduced by laser phase noise and frequency offset in pilot carrier-assisted direct detection scheme [7, 10], when the pilot carrier and optical DMT signal are beating in the PD. Conventionally, the phase noise needs to be compensated after fast Fourier transform (FFT) demodulation of DMT signal, based on pilots inserted in each DMT symbol [13]. However, such a method is only effective when the laser linewidth is small with the assumption that the phase noise is constant over one DMT symbol period. Therefore, conventional method cannot function well, especially when the laser linewidth is large, which introduces strong inter-carrier interference among subcarriers in one DMT symbol. In order to solve this issue, PPC has been proposed to extract the variation of phase noise directly before FFT demodulation [8, 9]. The conceptual heart of PPC is to extract the low frequency part of the DMT signal, which can realize accurate tracking of the phase noise in frequency domain. The PPC method can be very effective for DMT signal, especially when the low-frequency region may contain no useful information via subcarrier mapping. The optical spectrum of DMT signal without and with laser phase noise is shown in Fig. 1(a) and (b), respectively. It is observed that, the frequency spectrum is broadened in the low-frequency region when laser phase noise is added to the DMT signal. Please note that the low frequency components always exist in optical spectrum of DMT signal, because the direct current (DC) component cannot be perfectly removed during the electrical-to-optical conversion. Here, we define the input signal to the PPC block as vector $\boldsymbol{R}_{in}$ with a length of M. Conventional PPC [8, 9] can be described in Fig. 2(a) as:

(1) Taking the FFT to the whole vector $\boldsymbol{R}_{in}$ and extracting the low-frequency values in the frequency domain to represent the phase noise information as vector **L** with a length of N_0;

(2) Defining a new all zeros vector **P** with a length of M and then setting the corresponding N_0 low-frequency elements with vector **L**;

(3) Taking the IFFT to the vector **P** to obtain the time-domain phase noise information, represented by vector **T** with a length of M;

(4) Normalizing the vector **T** and dot multiplying by the vector $\boldsymbol{R}_{in}$ to obtain the output signal after PPC, represented by the vector $\boldsymbol{R}_{out}$.

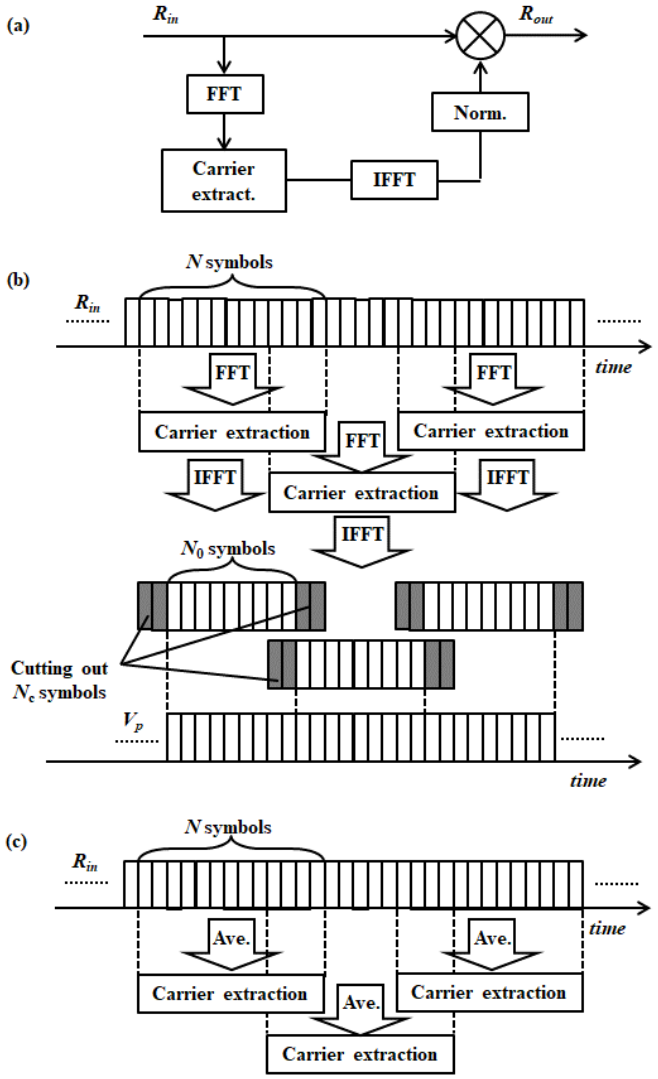

Fig. 2 (a) Pre-phase compensation scheme; (b) Low-complexity carrier phase estimation based on overlap frequency domain estimation; (c) Simplified carrier phase extraction scheme without requirement of FFT and IFFT.

For conventional PPC [8, 9], FFT with large size is indispensable to extract the phase information, which increases the computational complexity in a large degree. In order to

reduce the computational complexity, we propose an overlap frequency domain estimation (OFDE) algorithm to estimate the phase variations, which is similar to overlap frequency domain equalization algorithm for digital CD compensation [14]. First, FFT is performed on the N samples of the signal, instead of the whole M samples. Then the carrier phase information represented by several samples is directly extracted in frequency domain. In order to maintain the same length of N in both frequency and time domains, the frequency-domain carrier phase information is presented by a $N\times1$ vector. The carrier phase information in frequency domain is located in the low frequency region and the values in the high frequency region are set to zero. After inverse FFT (IFFT), the first N_c symbols and the last N_c symbols within the N symbols are removed, as shown in Fig. 2(b). The remaining N_0 ($= N - 2N_c$) symbols are finally extracted. Therefore, the phase noise of the whole signal can be continuously estimated which is performed at the overlapped FFT block and shifted by N_0 symbols. According to the above descriptions, conventional PPC can be regarded as a special case in our proposed method, when we extract the frequency-domain carrier phase information directly by taking the FFT to the whole length of signal [8, 9].

Regarding the computational complexity of PPC, we assume the length of signal M is 2^m and the FFT size N is 2^n. Conventional PPC may carry out the FFT and IFFT for the entire length of M, which results in the number of complex multipliers as $M \cdot log_2 M\ (= m \cdot 2^m)$. However, the number can be expressed as $\left\lceil \frac{M}{N-2N_c} \right\rceil \cdot N \cdot log_2 N$ for our proposed method, where $\lceil X \rceil$ represents the operation to round the elements of X to the nearest integers towards infinity. For simplicity, we assume $N - 2N_c \geq N/2$. Therefore, the upper bound of the number of complex multipliers can be expressed as $M/(N/2) \bullet N \bullet log_2 N\ (= 2n \bullet 2^m)$. In such a case, the computational complexity can be reduced under the condition of $n < m/2$. It is also noted that not all the samples in the frequency domain are extracted as the carrier phase information for the PPC process. If the FFT size is small, only a small number of samples after FFT are required to extract the carrier phase information. Specifically, if only one sample is required, no complex multipliers are required since simply averaging all samples with the length of FFT size can help the carrier information be extracted. Since the FFT and IFFT matrices are orthogonal, the IFFT operation can be simplified without requiring complex multiplication. Thus, the carrier phase can be directly extracted in time domain. The operations of FFT and IFFT are simply replaced by the averaging operation. The corresponding simplified carrier phase extraction process is shown in Fig. 2(c). Please note that the moving average filter solution for carrier phase extraction of orthogonal frequency division multiplexing (OFDM) signal [15] is also a special case of our proposed DSP scheme, when the shift number N_0 is 1.

In order to accurately evaluate the effectiveness of our proposed method, we design the channel model of pilot carrier-assisted DMT signal transmission with direct detection as shown in Fig. 3(a). The effects of laser phase noise and frequency offset are emulated by multiplying with the real-valued DMT signal in the channel model. The additive white Gaussian noise (AWGN) is added on both real and imaginary parts. The direct detection implementation is modelled by the square operation. Therefore, the received signal is real-valued and expected to be positive. Based on the channel model in Fig. 3(a), the corresponding simulation setup is shown in Fig. 3(b). The DMT signal is generated with sampling rate of 64GSa/s, FFT size of 256, payload subcarrier number of 66, cyclic prefix (CP) length of 8, and 16 quadrature amplitude modulation (16-QAM) format. The frequency offset between two lasers is 30 GHz. The laser linewidth is set to 1 MHz, and the laser phase noise is modeled as Wiener process [16]. The power ratio between the local oscillator (LO) and signal is set to be 20 dB to mitigate the effects of signal-to-signal beating noise (SSBN).

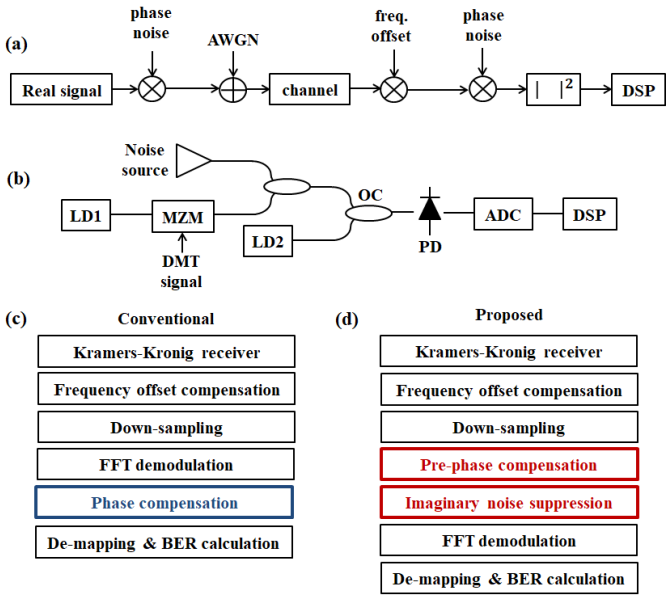

Fig. 3 (a) Channel model of pilot carrier-assisted DMT signal transmission with phase noise and AWGN; (b) Simulation setup for the pilot carrier-assisted DMT signal detection scheme; (c) Conventional and (d) Proposed DSP flows for the DMT signal recovery.

In the simulation, two DSP methods with and without PPC for DMT signal are numerically compared, as shown in Fig. 3(c) and (d). Most of DSP flows are the same for both methods including the Kramers-Kronig (KK) receiver, frequency offset compensation (FOC), down-sampling, FFT demodulation, symbol de-mapping and bit error rate (BER) calculation. It is noted that the signal becomes complex-valued after FOC, when the signal spectrum is no longer symmetrically conjugated. The main difference between the two DSP flows is the order of phase noise compensation. For the conventional method, the phase noise compensation is performed after the FFT demodulation in frequency domain. Data-aided phase noise compensation is applied in the simulation, with the assumption that all transmission data are known in each DMT symbol [13]. However, our proposed DSP flow performs the phase noise compensation in time domain before the FFT demodulation. It is also noted that we propose to remove the imaginary part of the signal after PPC as shown in Fig. 3(d). This is mainly because the main signal energy is located in the real part of the

signal after PPC and the imaginary part only contains noise. Please note that the DMT signal after FFT demodulation is complex-valued, no matter whether the DMT signal is real-valued or complex-valued before FFT demodulation. Therefore, half of the noise is expected to be mitigated in time domain, due to the removal of the imaginary part of signal before the FFT demodulation. Moreover, AWGN mitigation can also be achieved in frequency domain when the Hermitian symmetry property of the Fourier transform is explored as $\bar{X}(f) = 1/2 \times [X(f) + X^*(-f)]$, where $X(f)$ and $\bar{X}(f)$ are the symbols at frequency f before and after AWGN mitigation, and $X^*(-f)$ is the conjugated symbol at frequency $-f$ before AWGN mitigation.

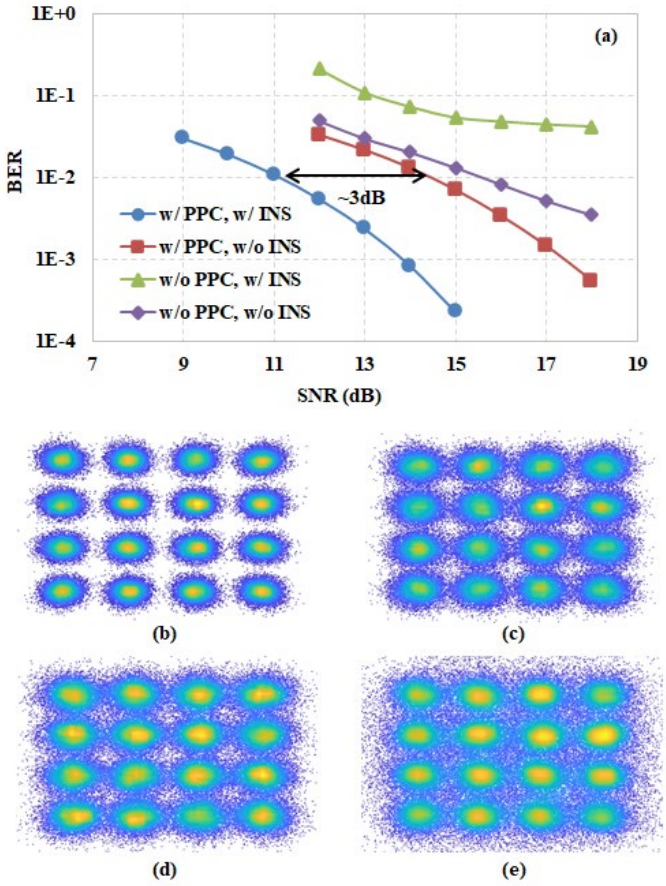

Fig. 4 (a) BER performance comparisons of pilot carrier-assisted DMT signal detection with or without PPC/INS. Signal constellation at SNR of 15dB (b) with PPC and with INS; (c) with PPC and without INS; (d) without PPC and without INS; (e) without PPC and with INS.

We first evaluate the function of PPC and INS under conditions of four scenarios (with or without PPC/INS). As for our proposed PPC scheme, the FFT size N and the removed number N_c are set to be 64 and 8, respectively. Only one sample is extracted in frequency domain to represent the carrier phase information. The BER performance with respect to signal-to-noise ratio (SNR) is presented in Fig. 4(a). It is observed that PPC combined with INS can improve the SNR by ~3 dB in comparison with the case of with PPC but without INS. According to the channel model in Fig. 3(a), the signal information is actually encoded in the real part and a certain amount of signal energy is transferred into imaginary part, due to the beating between signal and pilot at the PD. The imaginary part of the complex signal includes both signal energy and imaginary part of AWGN. In such a case, if the phase noise is pre-compensated in time domain for DMT signal, it can be assumed that all useful signal information is located in the real part of the complex signal. Removal of the imaginary part of the signal means the reduction of noise power by ~3 dB. Therefore, the simulation result in Fig. 4(a) agrees well with above theoretical explanations. It is also observed in Fig. 4(a) that INS operation may degrade the performance, if PPC is not applied in advance. This is mainly because the imaginary part of the signal may also contain useful information if the laser phase noise is not mitigated. The constellation points for the four cases at SNR of 15 dB are also shown in Fig. 4(b)-(e). As shown in Fig. 4(e), the constellation points of the recovered signal are seriously distorted, when the phase noise is not fully compensated before the INS operation.

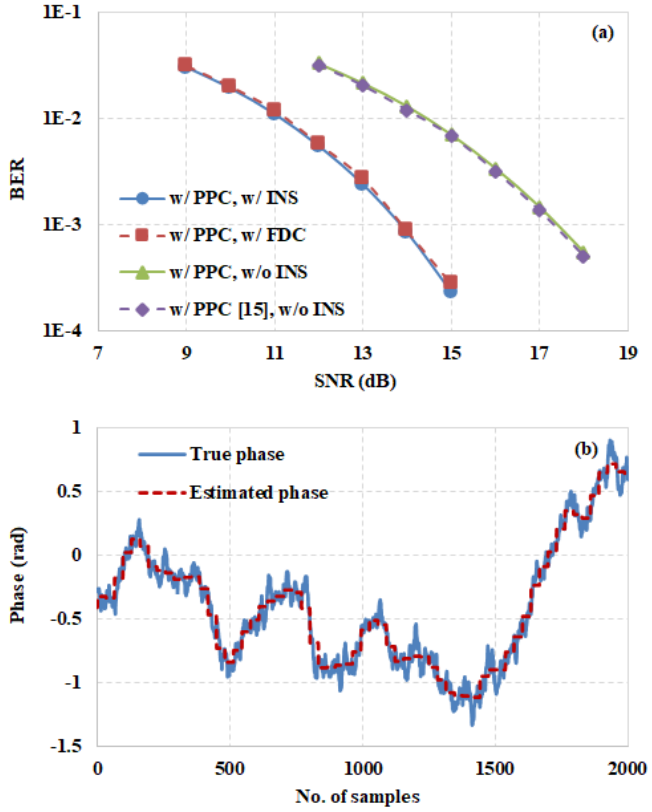

Fig. 5 (a) BER performance comparisons of pilot carrier-assisted DMT signal detection with different schemes for PPC and AWGN mitigation; (b) Estimated and true phase values under the condition of 1 MHz linewidth.

Next, we investigate the performance of frequency domain conjugation (FDC) method for the AWGN mitigation. As shown in Fig. 5(a), FDC has similar performance as INS after PPC. However, the FDC method has to process the data at the negative frequency region. Therefore, the required computation complexity is doubled during the channel equalization process in comparison with the use of INS method. The performance of INS method is similar to that of FDC method, but lower computational complexity, we prefer to use INS method in the future study. It is al`so noted that both FDC and INS methods are not suitable for conventional direct detection of DMT signal

[11], when the digital signal is processed only in real-valued domain.

Finally, we investigate the function of PPC based on our proposed scheme and scheme in [15] without requiring complex multiplier operations. As for the PPC scheme [15], the average number is set to 64. As shown in Fig. 5(a), we can observe similar performances for both schemes. However, the shift number of our proposed PPC scheme is much larger than 1, which means that our proposed PPC scheme is ideally for parallel signal processing, for the purpose of latency reduction. Moreover, we also provide the estimated phase values in Fig. 5(b) under the condition of 1 MHz linewidth. We can observe that the values of the estimated phase agree well with that of the true phase.

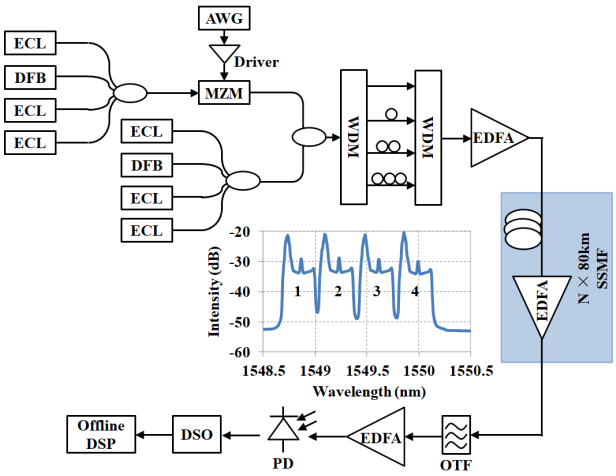

Fig. 6 Experimental setup of 4×50-Gb/s DMT signal transmission based on pilot carrier-assisted direct detection scheme. Inset: optical spectrum at the output of WDM. ECL: External cavity laser, DFB: distributed feedback, MZM: Mach-Zehnder modulator, WDM: wavelength division multiplexer, EDFA: Erbium doped fiber amplifier, SSMF; standard single mode fiber, OTF: optical tunable filter, PD: photodetection, DSO: digital oscilloscope.

III. Experimental Setup

Fig. 6 shows the experimental setup for the transmission of 4×50-Gb/s DMT signal combined with pilot carriers over 400-km SSMF. At the transmitter side, four laser sources at channel spacing of 50 GHz are combined by an optical coupler (OC). One of four laser sources is a distributed feedback (DFB) laser with a linewidth of ~10MHz. The other three laser sources are external cavity lasers (ECLs). The digital DMT signal is generated offline and then sent to an arbitrary waveform generator (AWG) operating at 64 GSa/s. The FFT size is 256, where the first 3 subcarriers are used as a guard band. The following 66 subcarriers are loaded with data in 16-QAM format. Hermitian symmetry is applied to realize the real-valued signal. 1/32 of the FFT size is used as CP to avoid the inter-symbol interference. Considering the forward error correction (FEC) code with 20% overhead, the net data rate per wavelength can be calculated as 64GSa/s × 66 /(256 + 256/32) × log2(16b/Sa)/1.2 = ~50Gb/s. The analog DMT signal from the output of AWG is then modulated onto the MZM, which is biased with a small offset to the null point for power efficient transmission [8, 9]. Please note that if the RF pilot is inserted in the DMT signal, the real-valued signal cannot be generated. Another four laser carrier sources are also combined by an OC at channel spacing of 50 GHz. In order to achieve direct detection, the center frequency of laser carrier source is shifted by 16 GHz to that of the corresponding optical DMT signals. The four optical DMT signals and their corresponding laser carrier sources are finally combined via another OC to achieve four-channel pilot carrier-assisted optical signals. To decorrelate the four-channel optical signal, the combined optical signals are first demultiplexed by one wavelength-division multiplexer (WDM) followed by four pieces of SSMF and then re-combined by another WDM. The spectrum of optical signals at the transmitter side is also shown in the inset of Fig. 6. The small peaks in the middle of each DMT signal are also observed, which agree well with the simulated spectrum in Fig. 1. The transmission link includes several spans of 80-km SSMF with the transmission loss compensated by Erbium doped fiber amplifier (EDFA) for each span.

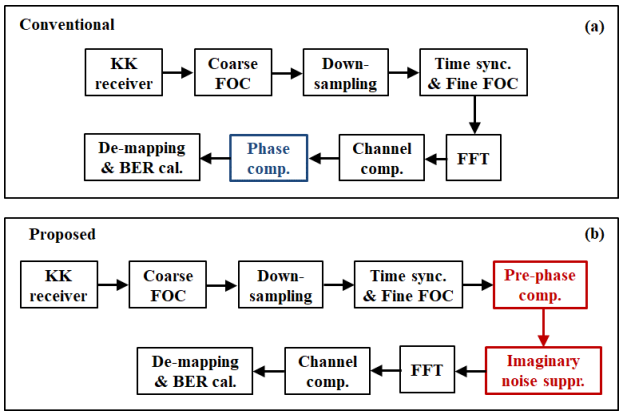

Fig. 7 DSP flows based on (a) conventional method and (b) proposed method with low-complexity pre-phase compensation and imaginary noise suppression.

At the receiver side, an optical tunable filter (OTF) is used to select the desired channel and another EDFA is used to adjust the received optical power. The optical-to-electrical conversion is achieved by a photodetector (PD) with a bandwidth of 40 GHz. Then, analog-to-digit conversion is achieved by a digital sampling oscilloscope (DSO) at a sampling rate of 160 GSa/s with a bandwidth of 59 GHz. Finally, the digitized signal is processed offline. During the offline DSP, the steps of two DSP flows are shown in Fig. 7. For both cases, a normal Kramers-Kronig receiver is first applied to mitigate the effect of SSBN. Then a coarse FOC is performed, followed by down-sampling of the received signal to 1 sample/symbol. The process of coarse FOC for the n^{th} sample of the received signal $\mathbf{x}$ can be expressed as $\mathbf{y}(n) = \mathbf{x}(n) \times \exp(j \cdot \Delta f \cdot \Delta t \cdot n)$, where $\mathbf{y}(n)$ presents the n^{th} sample of signal after coarse FOC, Δf is the value of coarse frequency offset (16GHz in our experimental demonstration) and Δt is the sampling interval (1/160G in our experimental demonstration). Next, the time synchronization and fine FOC can be then achieved in a way similar to the conventional OFDM with a number of specifically designed training sequences generated at the transmitter side [17]. Like the simulation case, the main difference between two DSP flows is still the order of phase noise compensation, as shown

in Fig. 7. For simplicity, we test the performance of the received signals in channel 2 and channel 3 (inset of Fig. 6), where two pairs of ECLs and DFB lasers are used as signal and pilot carriers, respectively. About 2 million bits are collected to calculate the BER during the experimental demonstration.

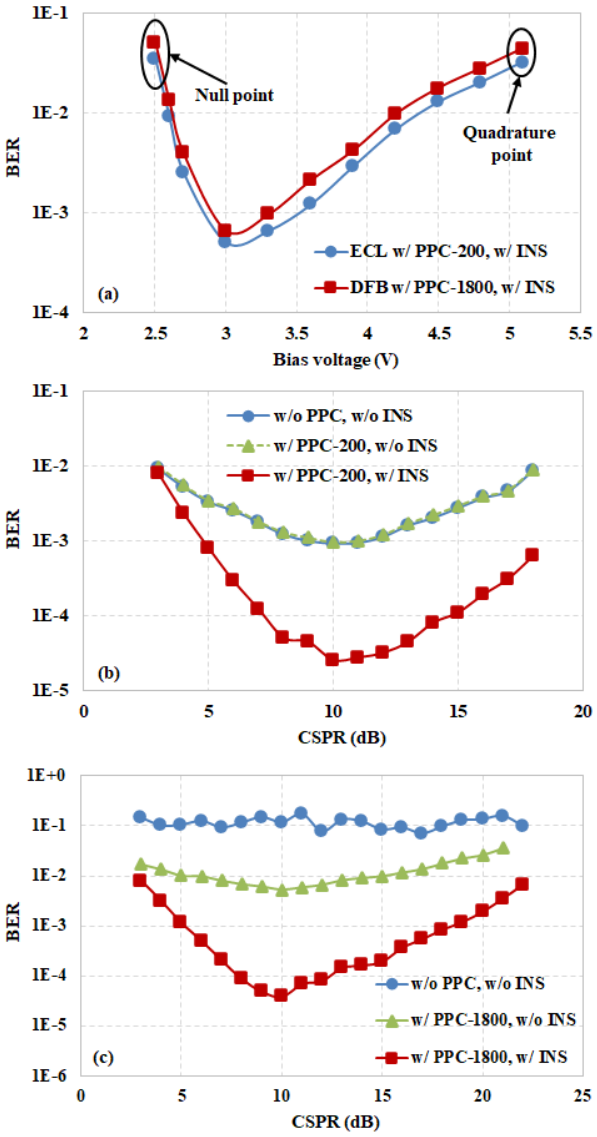

Fig. 8 BER performances under the condition of back-to-back versus (a) bias voltage, (b) CSPR for ECL pairs and (c) CSPR for DFB pairs.

IV. Results and Discussion

For the BER performance evaluation, we first specify the parameters in our proposed method as FFT size, overlapped samples and extracted samples for the carrier phase estimation. For example, PPC-(128, 16, 1) means the FFT (or averaging) size is 128, and the overlapped samples is 16 with only one extracted sample. If FFT size M (M = 262144) is equal to the whole number of samples, only the number of the extracted samples is considered here. For example, PPC-200 means 200 low-frequency samples (N_0 = 200) are extracted in frequency domain to present the phase noise. For the conventional phase estimation method [13], we insert 4 pilot subcarriers in each DMT symbol before applying the decision-aided and decision feedback phase estimation technique [18].

We first identify the optimal bias point of MZM under the condition of back-to-back transmission, when the OSNR is set to 25 dB. For the ease of discussion, we assume that the FFT size is equal to the number of samples. Thus, both 200 and 1800 samples are extracted in frequency domain in order to represent the carrier phase information for ECL and DFB laser pairs, respectively. The number of the extracted samples is different for ECL and DFB lasers, due to their different laser linewidths. As shown in Fig. 8(a), the BER performance is improved when the bias point of MZM is ~3V for both ECL and DFB laser pairs. It is also noted that the bias point is very close to the null point. However, the BER performance degrades fast, when the bias point is approaching the null point. This is mainly because the phase information cannot be accurately extracted if the bias point is set at the null point.

Then we investigate the effects of carrier-to-signal power ratio (CSPR). In order to verify the function of PPC and INS, we also consider the case with PPC but without INS. As shown in Fig. 8(b), when the signal and pilot lasers are ECLs, the proposed method shows better performance than the conventional method. However, if only PPC is applied, no performance improvement is observed, which is mainly because the laser phase noise is small when the ECL laser is used. However, when a pair of DFB lasers is used, our proposed method shows much higher performance improvement than that of the conventional method. As shown in Fig. 8(c), the signal cannot be successfully recovered with the help of the conventional method. The performance improvement of PPC is also observed, when the laser phase noise is large. From the results in Fig. 8, the value of CSPR is fixed to be 10 dB for the future experimental demonstrations.

Next, we investigate the OSNR performance with our proposed and conventional methods under the condition of back-to-back transmission. From Fig. 9(a) and (b), we can observe that our proposed method shows much better performance improvement than that of conventional method. Similar to the results in Fig. 8, PPC is also only valid when the laser phase noise is large. The BER floor is observed in Fig. 9, because of excessive impairments like nonlinear distortions in the electrical driver, quantization noise in AWG and DSO, or thermal noise in PD.

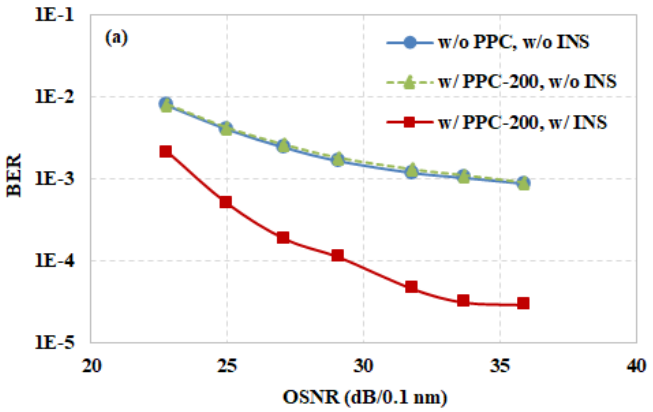

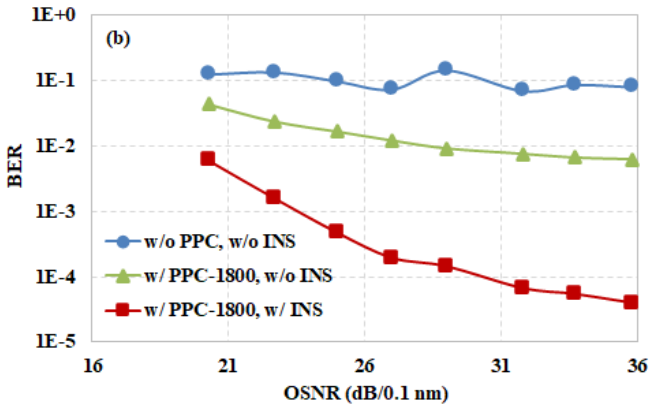

Fig. 9 OSNR versus BER at back-to-back case for (a) ECLs; (b) DFB lasers.

We also investigate the effects of parameters in our proposed low-complexity PPC algorithm. For fair comparison, we also consider the complex multiplier-free PPC scheme with average size of 128 proposed in [15]. From Fig. 10(a) and (b), we can see that the performance penalty is negligible when only one sample is extracted in the time domain with the averaging size of 128 representing the laser phase noise information in the time domain. The parameter set of (128, 16, 1) is chosen for the next fiber optical transmission investigation.

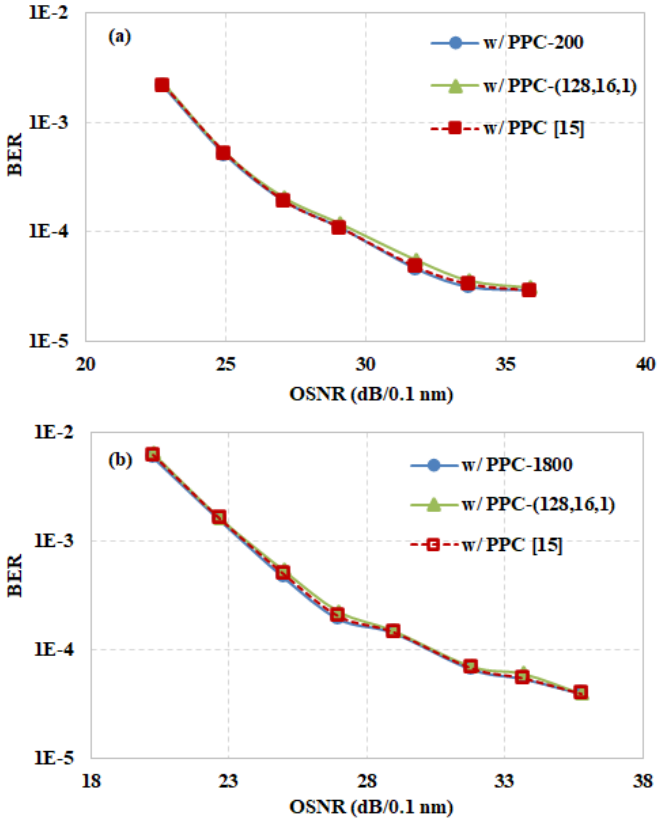

Fig. 10 OSNR versus BER at back-to-back case for (a) proposed method with different parameters and ECLs; (b) proposed method with different parameters and DFB lasers.

The launch power versus the BER performance for the transmission of 4×50-Gb/s DMT signal over 400-km SSMF is investigated, as shown in Fig. 11. Similar to the back-to-back case, the proposed method proves to perform more satisfactorily than the conventional method. The signal cannot be recovered with severe phase noise and without the help of PPC. Based on our proposed method, the BER of 4×50-Gb/s DMT signal after 400-km SSMF transmission is below the 20% FEC threshold (2×10^{-2}) with a sufficient margin for both ECL and DFB laser pairs. In our view, the computational complexities of our proposed PPC scheme and PPC scheme in [15] are similar in terms of complex multiplier operations. However, our proposed PPC scheme outperforms the PPC scheme in [15] by two ways. The first one is that our proposed PPC scheme requires much less addition operations, because the estimated phase is assumed to be a constant over consecutive samples with a length of N_0. It is noted that N_0 is always smaller than the number of subcarriers, but larger than 1. Therefore, the required number of addition operations per OFDM symbol based on our proposed PPC scheme is only $1/N_0$ of that based on PPC scheme in [15], where N_0 is 96 for our experimental demonstration. The second advantage is that our proposed PPC scheme can be implemented in parallel structure, because of large shift number, leading to less latency in the DSP.

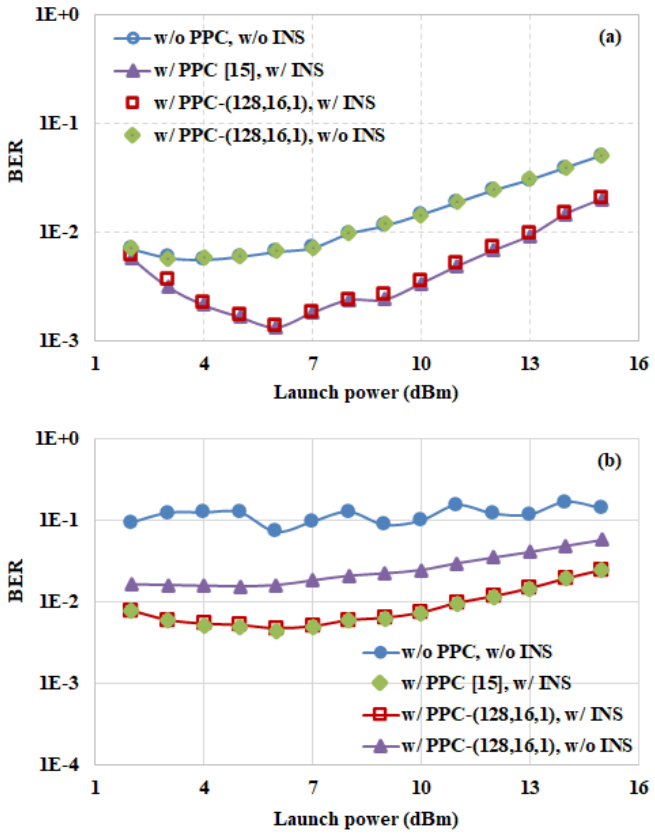

Fig. 11 Launch power versus BER after 400-km SSMF transmission with (a) ECLs and (b) DFB lasers.

In order to better observe the performance penalty during the fiber optical transmission, we evaluate the BER performances versus the transmission distance for the ECL and DFB pairs, respectively. As shown in Fig. 12(a), the maximal transmission distance can be more than 560 km at BER threshold of 0.02 for ECL pairs at optimal launch power of 6 dBm. Alternatively, as shown in Fig. 12(b), the maximal transmission distances for

DFB pairs are reduced to be ~480 km. This is mainly because the enhancement of phase noise reduces the accuracy of phase noise estimation. Considering the results of the back-to-back transmission and after the fiber optical transmission in Fig. 9 and Fig. 11, the performance penalty of fiber optical transmission is mainly caused by phase-to-amplitude noise conversion in the pilot-assisted direct detection transmission systems [19]. The constellation points at transmission distance of 400 km are also shown in Fig. 12.

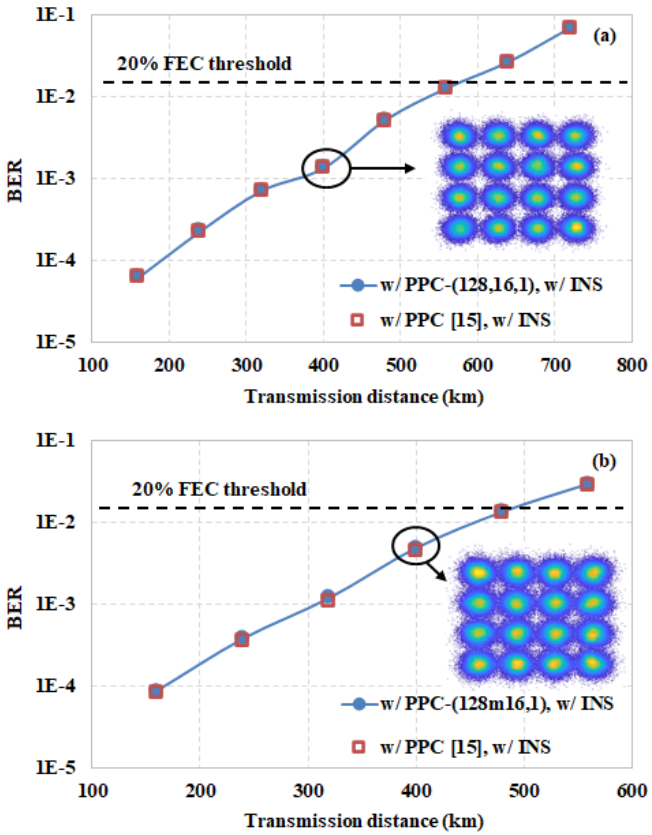

Fig. 12 BER performances versus transmission distance at launch power of 6 dBm for (a) ECL pair and (b) DFB pair.

V. Conclusion

We have experimentally demonstrated a cost-effective pilot-assisted DMT signal transmission system. A low-complexity PPC algorithm combined with INS is proposed to improve the performance when low-cost DFB laser is used. The phase noise of DMT signal can be pre-compensated in parallel before the FFT demodulation without requirement of additional complex multipliers. In comparison with conventional method, the experimental results show that INS can reduce the noise power, leading to the SNR improvement. Moreover, the DMT signal with severe phase noise cannot be recovered without PPC, due to the use of DFB laser with large linewidth. Finally, we have successfully demonstrated 4×50 Gb/s DMT signal transmission over 400-km SSMF using DFB lasers as optical and pilot carriers, which has the potential applications for future cost-effective metro networks.

References

[1] G. N. Liu, L. Zhang, T. Zuo, and Q. Zhang, "IM/DD transmission techniques for emerging 5G fronthaul, DCI and metro applications," J. Lightwave Technol., vol. 36, no. 2, pp. 560-567, Jan. 2018.

[2] K. Zhong, X. Zhou, J. Huo, C. Yu, C. Lu, and A. P. T. Lau, "Digital signal processing for short-reach optical communications: a review of current technologies and future trends," J. Lightwave Technol., vol. 36, no. 2, pp. 377-400, Jan. 2018.

[3] S. Li, S. Ohlendorf, S. Pachnicke, "100 km 56 GBd PAM-4 transmission using photonic reservoir computing," Proc. European Conference on Optical Communication, Dublin, 2019, Tu.2.B.

[4] M. Presi, G. Cossu, G. Contestabile, E. Ciaramella, C. Antonelli, A. Mecozzi, M. Shtaif, "Transmission in 125-km SMF with 3.9 bit/s/Hz spectral efficiency using a single-drive MZM and a direct-detection Kramers-Kronig receiver without optical CD compensation," Proc. Optical Fiber Communication Conference, USA, 2018, Tu2D.3.

[5] S. T. Le, K. Schuh, F. Buchali, M. Chagnon, and H. Bulow, "1.6 Tbps WDM direct detection transmission with virtualcarrierover 1200 km," Proc. Optical Fiber Communication Conference, USA, 2018, Tu2D.5.

[6] Y. Zhu, M. Jiang, X. Ruan, C. Li, and F. Zhang, "16×112Gb/s Single-Sideband PAM4 WDM Transmission over 80km SSMF with Kramers-Kronig Receiver," Proc. Optical Fiber Communication Conference, USA, 2018, Tu2D.2.

[7] X. Li, M. Luo, C. Li, C. Yang, H. Li, and S. Yu, "Direct detection of pilot-assisted PAM-4 signals with large phase noise tolerance," Opt. Lett., vol. 44, no. 22, pp. 5457-5460, Nov. 2019.

[8] C. Li, R. Hu, Q. Yang, M. Luo, W. Li, and S. Yu, "Fading-free transmission of 124-Gb/s PDM-DMT signal over 100-km SSMF using digital carrier regeneration," Opt. Express, vol. 24, no. 2, pp. 817–824, Jan. 2016.

[9] C. Li, M. Luo, and X. Li, "4 × 128-Gb/s PDM-DMT signal transmission over 1440-km SSMF with high phase noise tolerance," Opt. Express, vol. 26, no. 23, pp. 30901-30910, Nov. 2018.

[10] C. Yang, M. Luo, C. Li, W. Li, and X. Li, "Transmission of 64-Gb/s pilot-assisted PAM-4 signal over 1440-km SSMF with phase noise mitigation", Photonics Journal, vol. 11, no. 1, pp. 7200709, Jan. 2019.

[11] T. Tanaka, M. Nishihara, T. Takahara, W. Yan, L. Li, Z. Tao, M. Matsuda, K. Takabayashi, and J. C. Rasmussen, "Experimental demonstration of 448-Gbps+ DMT transmission over 30-km SMF," Proc. Optical Fiber Communication Conference, USA, 2014, M2I.5.

[12] C. H. Yeh, C. W. Chow, H. Y. Chen, and Y. F. Wu, "10-Gbps OFDM upstream rate by using RSOA-ONU with seeding-light for 75 km long-reach PON access," Proc. Optical Fiber Communication Conference, USA, 2012, JTh2A.65.

[13] X. Yi, W. Shieh, and Y. Tang, "Phase estimation for coherent optical OFDM," IEEE Photonics Technology Letters, vol. 19, no. 12, pp. 919-921, June 2007.

[14] R. Kudo, T. Kobayashi, K. Ishihara, Y. Takatori, A. Sano, and Y. Miyamoto, "Coherent optical single carrier transmission using overlap frequency domain equalization for long-haul optical systems," J. Lightwave Technol., vol. 27, no. 16, pp. 3721-3728, Aug. 2009.

[15] W. Peng, T. Tsuritani and I. Morita, "Simple Carrier Recovery Approach for RF-Pilot-Assisted PDM-CO-OFDM Systems," J. Lightwave Technol., vol. 31, no. 15, pp. 2555-2564, Aug. 2013.

[16] I. B. Djordjevic, and T. Wang, "On the LDPC-coded modulation for ultra-high-speed optical transport in the presence of phase noise," Proc. Optical Fiber Communication Conference, USA, 2013, OM2B.1.

[17] H. Minn, V. K. Bhargava, and K. B. Letaief, "A robust timing and frequency synchronization for OFDM systems," IEEE Trans. Wireless Commun., vol. 2, no. 4, pp. 822-839, July 2003.

[18] S. Cao, P. Y. Kam, and C. Yu, "Decision-aided, pilot-aided, decision-feedback phase estimation for coherent optical OFDM systems," IEEE Photonics Technology Letters, vol. 24, no. 22, pp. 2067-2069, Nov. 2012.

[19] S. T. Le, K. Schuh, and H. N. Tan, "A closed-form expression for direct detection transmission systems with Kramers-Kronig receiver," IEEE Photonics Technology Letters, vol. 30, no. 23, pp. 2048-2051, Dec. 2018.